Sensitivity of Compact Polarimetric SAR Parameters to Modeled Lake Ice Growth

Mohammed Dabboor, *Member, IEEE*, and Mohammed Shokr, *Senior Member, IEEE*

***Abstract*— Synthetic aperture radar (SAR) is a valuable tool for lake ice monitoring. The recently proposed SAR configuration for Earth observation called compact polarimetric (CP) SAR could be a good compromised choice between conventional (single or dual) and fully polarimetric (FP) SAR for operational ice applications, including lake ice. Given its enhanced radar target information compared with conventional SAR systems over wider swath coverage compared with FP SAR, CP systems could play important role in the new generation of Earth observation systems. Herein, we study the evolution of CP SAR parameters from simulated CP SAR data in relation to early ice growth. Focus of the study is on four lakes located in Cornwallis Island, Canadian Central Arctic. We adopt parameters extracted from dual circular polarimetric and right circular transmit, linear (horizontal and vertical) receive configurations. In this study, we consider the ice thickness calculated from an established empirical model. Meteorological and ice climatological data were used to support the analysis. Results demonstrated a potential connection between a number of CP parameters and lake ice growth. Furthermore, we were able to highlight the relationship between the density of air bubbles in ice layer and the intensity of volume scattering mechanism, leading to the identification of lakes with increased gas production activities. Thus, differences between lakes in terms of density of air bubbles were detected and statistically evaluated.**

***Index Terms*— Bubble in lake ice, compact polarimetric (CP) synthetic aperture radar (SAR), ice thickness, lake ice.**

I. INTRODUCTION

IN JUNE 2019, the RADARSAT Constellation Mission (RCM) was launched as a follow-on to RADARSAT-1&-2 [1]. It is the evolution of the RADARSAT program of the Government of Canada, with new acquisition capabilities. The compact polarimetric (CP) synthetic aperture radar (SAR) configuration is a new RCM polarization acquisition option, in which a right circularly polarized radar signal is transmitted and two mutually coherent orthogonal (horizontal and vertical) linear polarizations are received [2]. The main advantage of such configuration is the increased radar target information in comparison with standard single and dual polarized SAR polarization options, while covering much greater swath widths compared with full polarimetric (FP) SAR polarization [3]. Therefore, the recently proposed CP SAR configuration for Earth observation could be a compromised choice for SAR applications [3].

Different studies have explored the potential of CP SAR imagery for Earth observation applications, such as sea ice mapping [4]–[7], mineral oil spill detection [8]–[10], wetland monitoring [11], [12], wind speed estimation [13]–[15], and significant ocean wave height estimation [16], [17].

Lakes are a characteristic of Arctic landscape, which contains tens of thousands of lakes with a wide variety of natural and human activities. Climate change has profound impacts on lakes in the Arctic region due to the recent global warming trend. Lake ice, in turn, impacts not only lake ecosystems but also regional weather events. Therefore, monitoring lake ice is necessary since changes in terms of its freezing and breakup dates, growth conditions, ice thickness, biological productivity, and migration of species that depend on ice-water status, all are directly related to impacts of climate change [18].

SAR remote sensing has become a valuable tool for lake ice monitoring, supporting predictions with numerical ice and weather forecasting systems. Different studies have investigated methodologies for lake ice classification [18]–[20], scattering mechanism investigation [21]–[23], and backscattering signature interpretation [24] using SAR imagery. However, quite limited studies in the international literature have investigated the potential of CP SAR imagery for lake ice monitoring. To our knowledge, only two studies in [25] and [26] investigated the potential of CP SAR imagery for lake ice freeze-up and breakup monitoring, respectively.

Therefore, the innovative aspect of our study lies in the fact that it is the first to study the sensitivity of time series-simulated CP SAR data driven by changes in the ice properties during the early ice growth. CP SAR data are simulated from a stack of time series FP RADARSAT-2 imagery, which was acquired over Cornwallis Island in the Canadian Central Arctic during the fall of 2017. A large set of CP parameters are extracted from the simulated CP SAR data and investigated for their sensitivity to lake ice growth. Our study is timely since the RCM became recently operational (late December 2019) and is currently passing the early-operation phase.

II. STUDY AREA AND SAR IMAGERY

We selected four lakes located in the southwest corner of Cornwallis Island (Fig. 1). Cornwallis Island is a polar desert

Manuscript received August 19, 2020; revised December 3, 2020; accepted December 23, 2020. Date of publication January 29, 2021; date of current version November 24, 2021. *(Corresponding author: Mohammed Dabboor.)*

Mohammed Dabboor is with the Science and Technology Branch, Environment and Climate Change Canada, Dorval, QC H9P 1J3, Canada (e-mail: mohammed.dabboor@canada.ca).

Mohammed Shokr is with the Science and Technology Branch, Environment and Climate Change Canada, Toronto, ON M3H 5T4, Canada (e-mail: Mohammed.Shokr@canada.ca).

Digital Object Identifier 10.1109/TGRS.2021.3050754

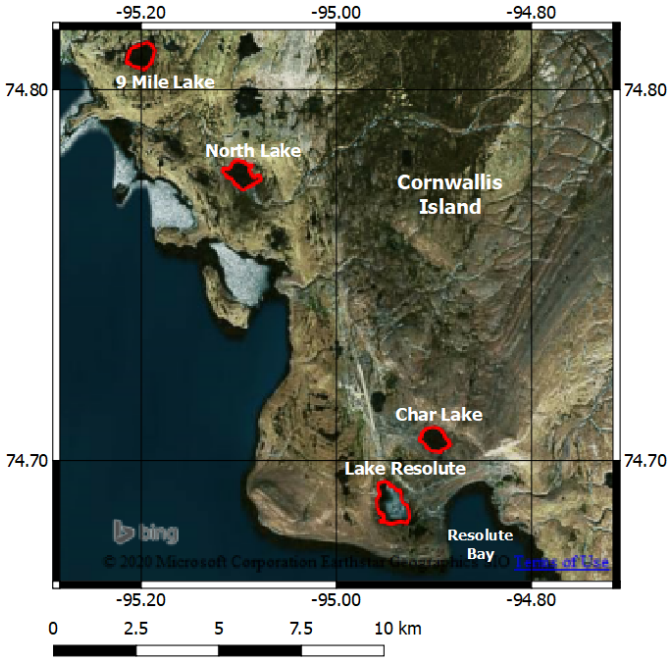

Fig. 1. Map of the study area. The inset shows the four lakes selected for the present study: Lake Resolute, Char Lake, North Lake, and 9 Mile Lake. Red polygons indicate selected lake samples.

island located in the Canadian Central Arctic. For the purpose of our study, we selected Lake Resolute, Char Lake, North Lake, and 9 Mile Lake (Fig. 1). All are deep lakes with an average depth equal to 22.5 m for Lake Resolute, 27.2 m for Char Lake, 20 m for North Lake, and 17.9 m for 9 Mile Lake [27]. Therefore, unlike shallow lakes, the four selected lakes are deep enough so that they do not freeze to the bottom in winter. North Lake is unique relatively to the other lakes in Cornwallis Island in the sense that it has the largest catchment area [27]. Moreover, field measurements in this lake reported 10–12 times higher concentrations of nitrate and nitrite when compared with all other major lakes in Cornwallis Island [27]. The higher concentrations of nitrate and nitrite in North Lake should lead to higher gas production activities compared with the other lakes, since denitrification of nitrate in lakes produces molecular nitrogen [28].

We acquired 62 Fine Quad Wide (FQW) RADARSAT-2 images over the selected lakes from 31 ascending overpasses of the satellite. Table I presents a summary of the acquisitions. Weather information for the present study was available from the Resolute Weather Station. This information included average daily air temperature, wind speed, and snow fall. Furthermore, site observations of ice development and environmental conditions were recorded by a resident operator at the upper air network (UAN) of Environment and Climate Change Canada (ECCC) at Resolute Bay. While field measurements of snow and ice properties, including thickness, would be crucial for our study, such data were not available because the study involved thin ice, and the period was on the verge then during the Arctic dark season. Furthermore, as confirmed by the UAN operator of ECCC, snow in this region is mostly drifted, which makes the distribution quite variable within short distances and timescales. The recorded information by the operator was made available for the purpose of our study.

TABLE I
SUMMARY OF THE RADARSAT-2 ACQUISITIONS SORTED BY THE BEAM MODE

Beam	Incidence angle		Date
	near	far	
FQ7W	24.9°	28.3°	20170927
FQ7W			20171021
FQ7W			20171114
FQ8W	26.1°	29.4°	20170920
FQ8W			20171014
FQ8W			20171107
FQ8W			20171201
FQ8W			20171225
FQ10W	28.4°	31.6°	20171007
FQ10W			20171031
FQ10W			20171218
FQ12W	30.6°	33.7°	20170930
FQ12W			20171024
FQ12W			20171117
FQ12W			20171211
FQ13W	31.7°	34.7°	20171110
FQ13W			20171204
FQ13W			20171228
FQ14W	32.7°	35.7°	20170923
FQ14W			20171017
FQ15W	33.7°	36.7°	20171010
FQ15W			20171103
FQ15W			20171127
FQ15W			20171221
FQ16W	34.8°	37.6°	20171003
FQ16W			20171120
FQ16W			20171214
FQ17W	35.7°	38.6°	20171027
FQ18W	36.7°	39.5°	20171123
FQ20W	38.6°	41.3°	20171130
FQ21W	39.5°	42.1°	20171207

III. DATA PROCESSING

Simulated CP SAR data was generated by a simulator using acquired RADARSAT-2 images. RADARSAT-2 imagery has extremely low noise floor better than −35 dB. The simulator converts the RADARSAT-2 16-bit complex products to 32-bit float complex by applying the provided sigma-nought calibration coefficients. Then, the RH (right circular transmit and linear horizontal receive) and RV (right circular transmit and linear vertical receive) polarizations are calculated from the calibrated HH, HV, VH, and VV polarizations. The RH and RV are converted to Stokes vector, which is then speckle filtered and used for the extraction of 22 CP parameters provided in Table II. Details on the calculation of these parameters were presented in [4]. The four lakes are sampled in the extracted CP parameters of each SAR image. One representative sample polygon covering the lake area is selected (red polygons in Fig. 1). Thus, time series of the mean values of the CP parameters in the four lakes are obtained by averaging the pixel values within each polygon. Sample polygons of Lake Resolute and Char Lake consist of 16 850 and 8825 pixels, respectively. For North Lake and 9 Mile Lake, the number of pixels is 8119 and 11 092 pixels, respectively.

TABLE II
ASSESSED PARAMETERS EXTRACTED FROM THE SIMULATED CP SAR DATA

Short form	Description
σ^0_{RH}, σ^0_{RV}, σ^0_{RR}, σ^0_{RL}	Sigma naught backscattering—right circular transmit and horizontal linear, vertical linear, right circular, or left circular receive polarization [4]
m-χ_V, m-χ_S, m-χ_DB	volume, surface, and double bounce scattering from m-χ decomposition [29]
m-δ_V, m-δ_S, m-δ_DB	volume, Surface, and double bounce scattering from m-δ decomposition [2]
SV0, SV1, SV2, SV3	Stokes vector elements [29][30] SV0: Total average received power. SV1: Received power in the linear horizontal (SV1 > 0) or vertical (SV1 < 0) polarized components. SV2: Received power in the linearly polarized at tilt angle 45° (SV2 > 0) or tilt angle 135° (SV2 < 0) components. SV3: Received power in left-circular (SV3 > 0) or right-circular (SV3 < 0) polarization.
SE_Pol, SE_Int	Shannon entropy polarimetric and intensity components [31]
μ	Conformity coefficient [32] [33]
m	Degree of polarization [29]
ρ_{RHRV}	RH RV correlation coefficient [4]
δ_{RHRV}	RH RV phase difference [3]
$\sigma^0_{RR}/\sigma^0_{RL}$	Circular polarization ratio [2]
α_s	Alpha feature related to the ellipticity of the compact scattered wave [32]

In our study, we apply the analysis of variance (ANOVA) test to examine if the difference between the obtained time series values of the CP parameters in the four lakes is significant by testing the following hypothesis [34]:

$$\begin{aligned} &H_0 : m_1 = m_2 = m_3 \ldots = m_k \\ &H_1 : \text{At least one mean is different} \end{aligned} \tag{1}$$

where k = the number of independent populations and m is the population mean. The ANOVA test procedure produces an F-statistic, which is used to calculate the p-value that indicates the probability that the null hypothesis is true. The null hypothesis examines if the true means of populations are equal against the alternative hypothesis that there is at least one inequality. We consider a significance level alpha = 0.05 for the test.

Given the lack of field measurements of ice thickness data, we consider a commonly used ice thickness empirical model for the calculation of the ice thickness of the four lakes. The model was proposed in [35]. This model corrects the simplest thermodynamic model for the presence of sensible heat loss, which is effective when the ice is thin and the difference between the temperatures of ice surface and air is large (more details are provided in [36]). Ice thickness h_i takes the following form:

$$h_i = \left[\frac{k_i}{\rho_i L_i}\text{FDD} + \left(\frac{k_i}{H_{ia}}\right)^2\right]^{0.5} - \left(\frac{k_i}{H_{ia}}\right). \tag{2}$$

The lake ice properties used in this equation are as follows; k_i is the thermal conductivity (2.25 J.m^{-1}s^{-1}K^{-1}), ρ_i is the density (917 kg.m^{-3}), L_i is the latent heat of fusion (334.9 kJ.kg^{-1}). FDD is freezing degree days and H_{ia} is a coefficient which accounts for the sensible heat flux from the ice surface to the air and depends on the wind speed. According to [35], a value of 20 is chosen to fit the nominal wind speed in the study area. Examination of the sensitivity of h_i to this parameter shows a constant difference of 2.3 cm between the two choices of H_{ia} = 18 and 20. This is a negligible difference for thick ice but not rightly so for thin ice, say <10 cm. Nevertheless, since the wind speed varies continuously over the ice cover, an average value of H_{ia} had to be selected. Moreover, in relating the CP parameters to the thickness of thin ice we are looking for the trend which is not affected by the choice of H_{ia}.

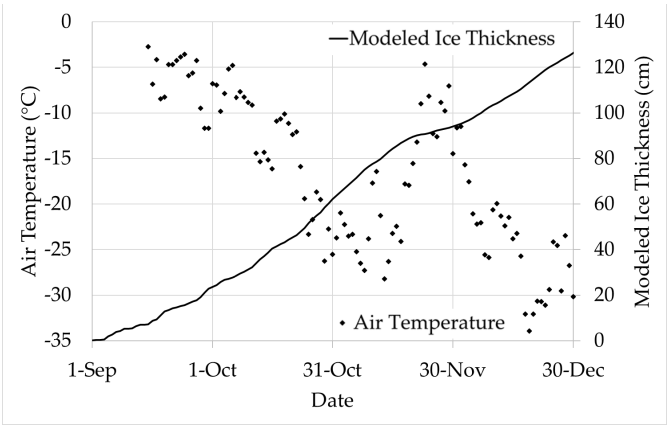

Fig. 2. Temporal evolution of the air temperature and the modeled ice thickness of lakes during the study period (September to December 2017).

The above model comes with uncertainty since it implies some assumptions about the ice, such as the snow-free ice surface. However, it is known that the C-band radar signal penetrates dry snow up to 2 m [37]. Two snow conditions would affect the radar signal: snow wetness and metamorphism (ice grains, crusting and change in density). Physical or empirical ice thickness model accounting for these two conditions would require accurate field measurements of those parameters as input, which were not feasible in our case, given the large study area, and the frequent snow drift causing highly variable spatial and temporal distributions of the snow. The weather station provides gross information about snow fall and its accumulation on ground. More information about the uncertainty of the used model for ice thickness estimation is presented in [35].

As provided in Table I, SAR images of our study were acquired from various imaging beam modes ranging from FQ7W to FQ21W. This reveals a maximum incidence angle difference between the centers of the images equal to 14.2°. The same SAR data set was used in [36], and the study has proved that the effect of the radar incidence angle difference is negligible (see [36, Fig. 2]).

IV. RESULTS AND DISCUSSION

A. Evolution of Air Temperature and Modeled Ice Thickness

As shown in Fig. 2, the air temperature reveals nearly monotonic decrease starting from the beginning of

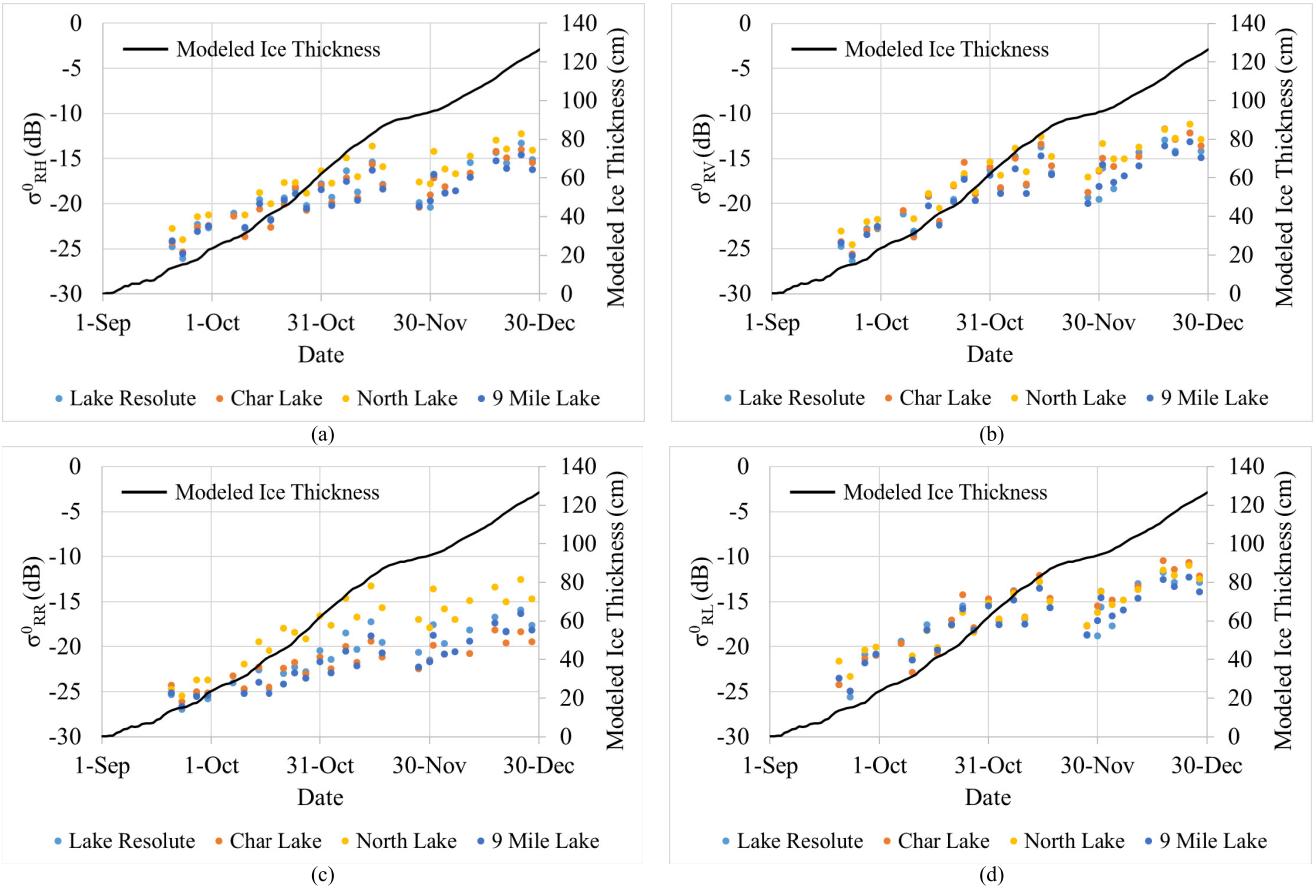

Fig. 3. Variation of modeled ice thickness and backscattering coefficients. (a) σ^0_{RH}, (b) σ^0_{RV}, (c) σ^0_{RR}, and (d) σ^0_{RL} during the ice growth.

September until about the mid of November. From the mid to the end of November, the air temperature increased to about $-4\,^{\circ}$C daily average before it resumed its decrease to the typical winter temperatures again.

The lakes started an uninterrupted freezing in the first week of September 2017 (Fig. 2). According to the ice thickness model in (2), the thickness increases as the air temperature decreases at an average rate of 1.1 cm/day. The rate slowed down during the period of air temperature increase between mid and end of November. The model shows that the lake ice thickness reaches the 127 cm by the end of December. While the thickness was not measured during the study period, it has been confirmed that it reached 2 m in Lake Resolute in May 2008 (Dr. Derek Muir, Personal Communication). Therefore, the calculated 127 cm by the end of December should be realistic.

B. Variation of CP Parameters Versus Modeled Ice Thickness

We analyze the evolution of the 22 simulated CP parameters against the calculated ice thickness for the four selected lakes.

1) Backscattering Coefficients: Plots of the evolution of the four backscattering coefficients σ^0_{RH}, σ^0_{RV}, σ^0_{RR}, and σ^0_{RL} with the modeled ice thickness of the four lakes are created and shown in Fig. 3. Moreover, statistics of the backscattering coefficients including the mean and the variance for the four lakes are presented in Table III. At the onset of freezing, the four backscattering coefficients assume low values (~ -27 dB) close to the backscattering from calm water. This is due to the reflection of the radar signal away from the radar antenna. These values increase monotonically in a relatively linear manner as the ice grows in the four lakes (Fig. 3). The increase of backscattering is attributed to the increasing density of air bubbles within the ice volume and the roughness of the ice–water interface. As the lake ice grows, the density of air bubbles within the ice volume increases, leading to increase of volume scattering. Moreover, surface scattering may be triggered by the roughness of the ice–water interface. These two factors are analytically explained in [23]. Similar results were observed in [36] for linear backscattering coefficients σ^0_{HH} and σ^0_{VV}.

Table III presents that for σ^0_{RH} the average backscattering ranges between -17.3 dB (North Lake) and -19.3 dB (9 Mile Lake). For σ^0_{RV}, it ranges between -16.7 dB (North Lake) and -18.5 dB (9 Mile Lake). Similar values are obtained for the dual circular polarizations. For σ^0_{RR} the range is between -17.7 dB (North Lake) and -21.9 dB (Char Lake), while for σ^0_{RL} it is between -16.4 dB (North Lake) and -17.2 dB (9 Mile Lake), respectively. Note that North Lake is consistently presenting the highest mean backscattering compared to the other lakes for all backscattering coefficients (Table III).

We note from Fig. 3(c) that the σ^0_{RR} backscattering coefficient is remarkably higher for North Lake, when compared with the other lakes. This is not the case for the σ^0_{RH},

TABLE III
STATISTICS OF THE BACKSCATTERING COEFFICIENTS WITH THE P-VALUE OF ANOVA TEST

		Lake Resolute (dB)	Char Lake (dB)	North Lake (dB)	9 Mile Lake (dB)
σ^0_{RH}	Mean	-19.0	-19.2	-17.3	-19.3
	variance	10.4	9.9	9.7	7.8
	P-Value	0.062			
σ^0_{RV}	Mean	-18.4	-17.7	-16.7	-18.5
	variance	14.5	15.6	13.9	12.1
	P-Value	0.303			
σ^0_{RR}	Mean	-21.2	-21.9	-17.7	-21.8
	variance	10.1	4.7	13.6	8.2
	P-Value	$2x10^{-6}$			
σ^0_{RL}	Mean	-17.1	-16.6	-16.4	-17.2
	variance	14.2	17.0	11.1	11.2
	P-Value	0.825			

σ^0_{RV}, and σ^0_{RL} coefficients. In order to confirm this observation statistically, we apply the ANOVA test [see (1)] to the four backscattering coefficients. The resulting p-value is presented in Table III for each backscattering coefficient. Considering a significance level alpha $= 0.05$, the p-value suggests that the difference in the average backscattering coefficient σ^0_{RR} from the four lakes is statistically significant ($2 \times 10^{-6} < 0.05$), leading to the rejection of the null hypothesis. This is not the case for the other backscattering coefficients, where the estimated p-value > 0.05, and therefore the null hypothesis is accepted (Table III). The ANOVA test indicates that a significant difference in σ^0_{RR} exists among the four lakes, but without specifying the different lakes. Therefore, in order to confirm that this significant difference is associated with North Lake, we reapply the ANOVA test to σ^0_{RR}, excluding North Lake. In this case, the resulting p-value $= 0.589$ (>0.05), stating acceptance of the null hypothesis that the difference in σ^0_{RR} backscattering from Lake Resolute, Char Lake, and 9 Mile Lake is not statistically significant. The statistically significant difference of σ^0_{RR} from North Lake should be triggered by an increased depolarization of the returned radar signal, which is analytically discussed in Section IV-B2. Finally, it is worth noting the effect of the increase in the air temperature around the mid to the end of November, which caused a drop in the backscattering values (ice thickness was around 90 cm), as shown in Fig. 3. This drop should be related to increased snow wetness following the increase in the air temperature, which limits the penetration of the radar signal and therefore reduces the scattering within the underlying ice layer [39]. The backscattering coefficients resume their increasing trend once the air temperature starts decreasing again.

2) Scattering Mechanisms: Herein, the variation of the three main scattering mechanisms: volume, surface, and double bounce calculated from the m-χ decomposition method is presented in Fig. 4. Moreover, statistics of the scattering mechanisms including the mean and the variance are presented for each lake in Table IV.

Air bubble inclusion is a characteristic of freshwater ice. Three types of bubbles exist: near the surface, within the volume, and near the bottom of the ice cover. Superimposed snow ice layer is usually formed on top of the ice sheet when wet snow or rainwater freezes. This layer has no connection to the underlying ice (the primary layer), and may grow from the bottom up and features small spherical bubbles with diameters ranging between sub-millimeters and a few millimeters [40]. Larger bubbles of tubular shapes exist within the main volume of lake ice. Here, large crystals (grains) are formed with fewer grain boundaries of ice grains, which are relatively far apart. As freezing progresses, the dissolved air in the lake water is pushed toward the boundaries, resulting in large-size bubbles of tubular shape following the orientation of the grain boundaries [40]–[42]. The above two bubble types trigger volume scattering with intensity that depends, among other factors, on the bubble size relative to the wavelength of the incident radar signal. The scattering increases as ice grows in response to the increasing number of air bubbles. With this, the extinction coefficient increases and the transmission coefficient decreases as analytically demonstrated in [23] using a radiative transfer model.

The third type of bubbles is found at the ice–water interface and usually observed in shallow waters [43]. As freezing progresses, gases that are dissolved in the lake water are pushed down until they saturate the underlying water. Only then, bubbles are rejected and incorporated into the ice near its water interface. In this scenario, bubbles contribute to the roughness of the ice–water interface. This contribution comes to add roughness triggered by the uneven ice growth to the ice–water interface, leading to an increasing surface scattering mechanism from the ice–water interface [23]. The surface scattering mechanism is caused by scattering off the bottom ice layer since portion of the radar signal penetrates the ice all the way to the ice–water interface. This is confirmed in a previous study of microwave scattering model [21]. It should be noted that the microwave dielectric mismatch is strong at the ice–water interface (3.15 F/m for ice and 80 F/m for water).

Fig. 4 reveals a visible linear increasing trend of both volume [Fig. 4(a)] and surface [Fig. 4(b)] scattering as the ice grows. We select, as example, North Lake to visually present the temporal increase in volume scattering during the study period [Fig. 5(a)–(d)]. For the temporal increase of surface scattering, Char Lake is selected [Fig. 5(e)–(h)]. As shown in both figures, volume and surface scattering mechanisms

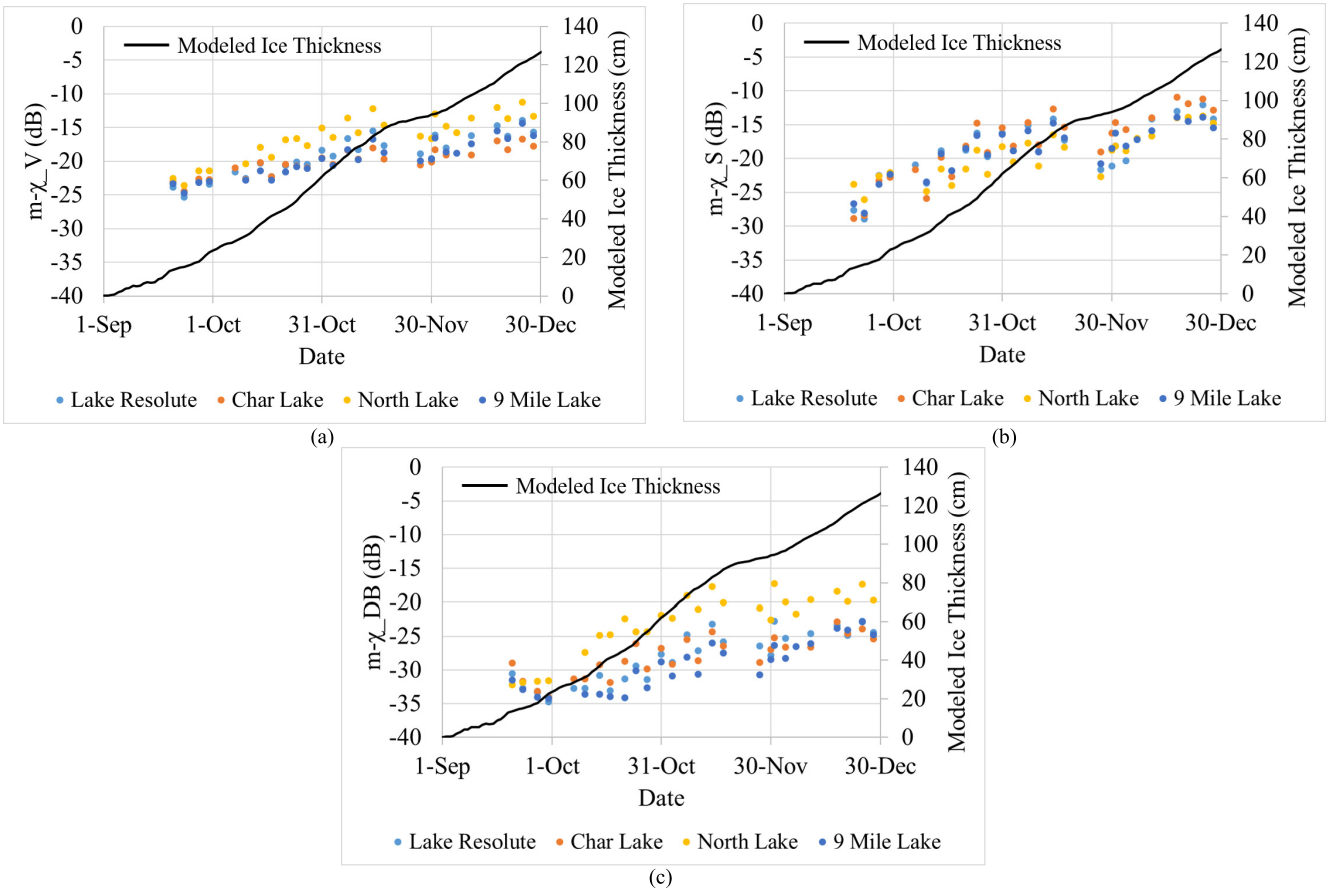

Fig. 4. Variation of the modeled ice thickness and (a) volume, (b) surface, and (c) double-bounce scattering mechanisms from the m-χ decomposition during the ice growth.

TABLE IV
STATISTICS OF THE SCATTERING MECHANISMS WITH THE P-VALUE OF ANOVA TEST

		Lake Resolute (dB)	Char Lake (dB)	North Lake (dB)	9 Mile Lake (dB)
m-χ_V	Mean	-19.2	-20.2	-16.4	-19.7
	variance	9.4	3.9	11.4	7.5
	P-Value	$2x10^{-5}$			
m-χ_S	Mean	-18.9	-17.9	-19.6	-18.7
	variance	18.3	25.6	12.2	14.3
	P-Value	0.582			
m-χ_DB	Mean	-28.2	-28.0	-22.9	-29.4
	variance	14.6	9.0	21.3	13.1
	P-Value	$4x10^{-8}$			

increase between September and December as the ice grows. The volume backscattering ranges between −16.4 dB (North Lake) and −20.2 dB (Char Lake). The surface scattering mechanism takes average values between −17.9 dB (Char Lake) and −19.6 dB (North Lake). Thus, North Lake records the highest average volume and the lowest average surface scattering mechanism.

Specifically for North Lake, we note that during the ice growth the volume scattering is remarkably higher than that of the other three lakes, as shown in Fig. 4(a). The higher volume scattering mechanism should be an indication of higher density of air bubbles of North Lake triggered by higher gas production activities. The assumption of higher gas production activities is linked to the higher concentrations of nitrate and nitrite in North Lake as reported from field measurements in [27]. A denitrification of the nitrate in lakes produces molecular nitrogen rather than nitrous or nitric oxides [28]. Therefore, we hypothesize that North Lake could be characterized by higher production of the nitrogen gas which causes higher density of air bubbles in its ice layer. These air bubbles are subsequently responsible for the higher volume scattering mechanism. This explains also the higher σ^0_{RR} backscattering coefficient [Fig. 3(c)] since both CP parameters are highly correlated [6]. In order to confirm that the difference of the volume scattering from North Lake is statistically significant, the ANOVA test is applied. As presented in Table IV, the derived p-value $= 2 \times 10^{-5}$, which is <0.05 (significance level alpha). Therefore, the null hypothesis that there is no significant difference in the volume scattering from the four lakes is rejected. However, by excluding North Lake the null hypothesis is accepted with p-value $= 0.414$. For the surface scattering the null hypothesis of the ANOVA test is accepted

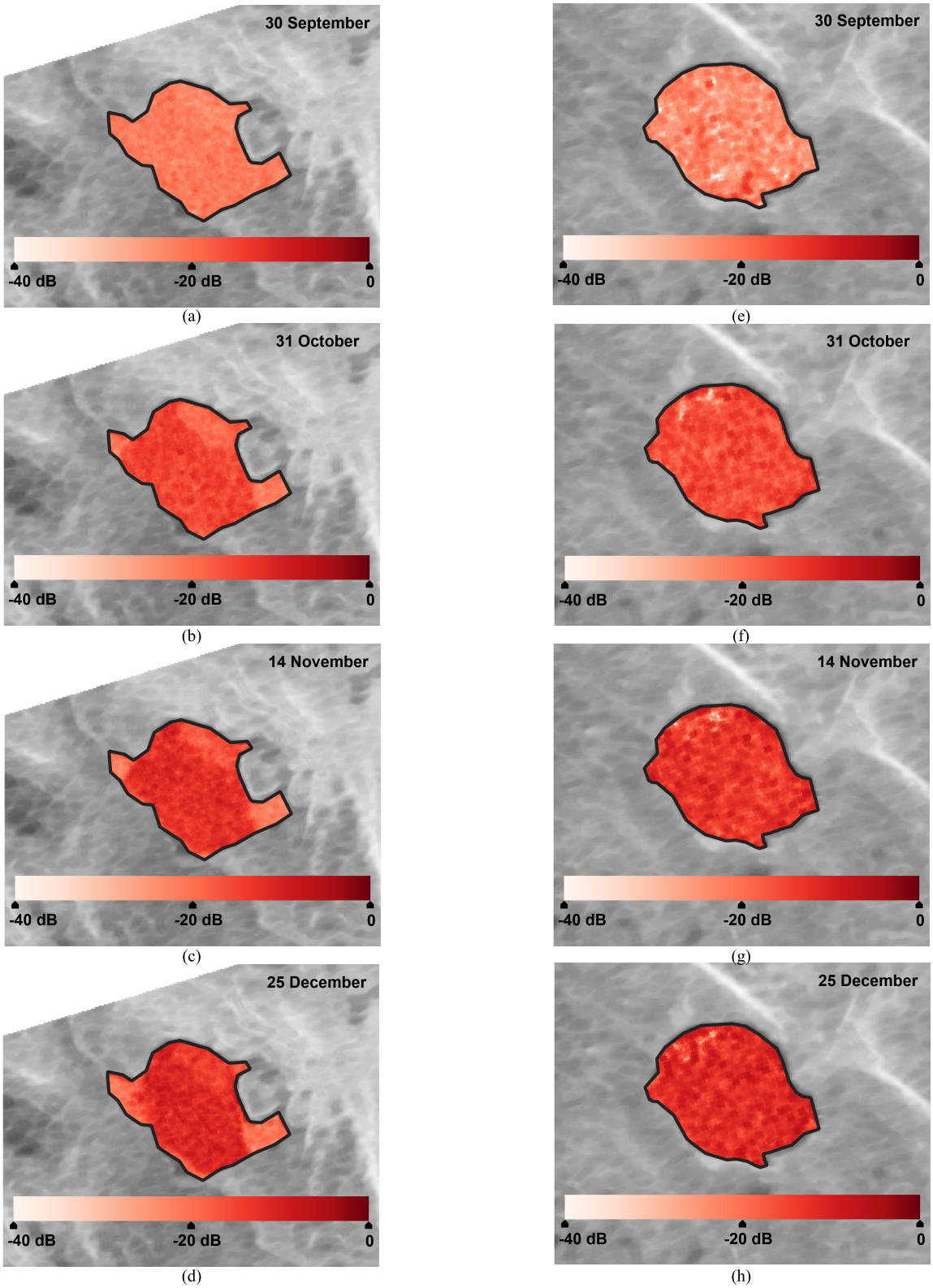

Fig. 5. Volume scattering mechanism from North Lake on (a) September 30, 2017, (b) October 31, 2017, (c) November 14, 2017, and (d) December 25, 2017. Surface scattering mechanism from Char Lake on (e) September 30, 2017, (f) October 31, 2017, (g) November 14, 2017, and (h) December 25, 2017. Background is the SPAN parameter from the image of 30 September 2017.

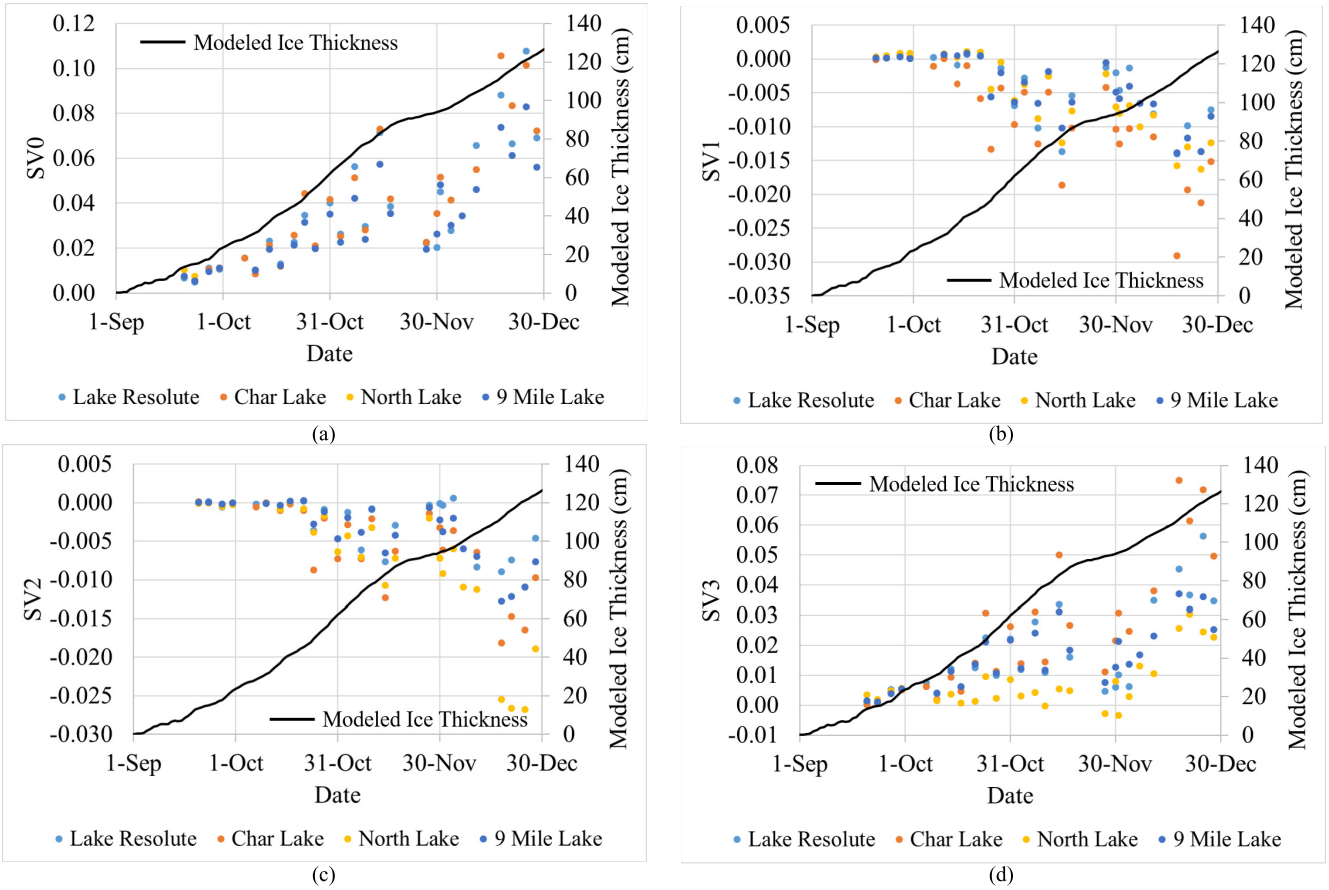

Fig. 6. Variation of the modeled ice thickness and Stokes vector elements. (a) SV0, (b) SV1, (c) SV2, and (d) SV3 during the ice growth.

at p-value $= 0.582$, indicating that there is no significant difference in the surface scattering mechanism from the lakes.

It is interesting to note that only for North Lake, the volume scattering mechanism [Fig. 4(a)] is consistently higher than the surface scattering mechanism [Fig. 4(b)] throughout the study period, with a difference between 0.1 and 6.5 dB. This is not the case for the other three lakes, since as the ice thickens the surface scattering mechanism becomes dominant, with an approximate average difference equal to -5 dB by the end of December [Fig. 4(a) and (b)]. These results agree with those presented in [22] for the dominancy of the surface scattering mechanism observed for mature thick lake ice in late fall.

As expected, double-bounce scattering mechanism is significantly lower than the other two mechanisms [Fig. 4(c)], though it presents a similar linear increasing tendency. This is confirmed from Table IV, where the mean of the double-bounce scattering is significantly lower than the mean of the volume and surface scattering mechanisms in each lake. Double-bounce scattering mechanism ranges between -22.9 dB (North Lake) and -29.4 dB (9 Mile Lake). This indicates the secondary contribution of this scattering mechanism in the backscattering process. This contribution could be associated with the backscattering scenario of the radar signal from columnar air bubbles then the ice–water interface. This is confirmed in previous results presented in [21] which show the limited contribution of the double-bounce mechanism in the scattering process, though the focus in that study was on shallow Arctic lakes. Note that the double-bounce scattering is remarkably higher for North Lake compared with the rest of the lakes (Fig. 4(c) and Table IV). This should confirm our previous interpretation about the higher density of air bubbles in the ice layer of North Lake, which should include increased columnar air bubbles causing a double-bounce scattering. Therefore, we apply the ANOVA test and examine the p-value to assess if the difference among the lakes in terms of double-bounce scattering is significant. As shown in Table IV, the null hypothesis of the ANOVA test is rejected at p-value $= 4 \times 10^{-8}$, indicating that there is a statistically significant difference in the double-bounce scattering mechanism from the lakes. In order to confirm that this difference comes from North Lake, we exclude it and reapply the ANOVA test. Herein, the null hypothesis is accepted with a p-value $= 0.294$ (>0.05).

Finally, it is worth noting that the effect of the increase in the air temperature during the mid to the end of November (ice thickness was around 90 cm) is visible in interrupting the linear trend, particularly in the surface scattering [Fig. 4(b)]. Given that the scattering mechanisms from the m-δ decomposition were found to provide results similar to the m-χ decomposition presented earlier, we limit our analysis to the m-χ decomposition to avoid information repetition.

3) Stokes Vector Elements: Variations of the four elements of the Stokes vector with the modeled lake ice growth are shown in Fig. 6. The mean and variance of the elements are presented in Table V. Interestingly, the four elements behave differently in relation to the lake ice growth. Unlike the

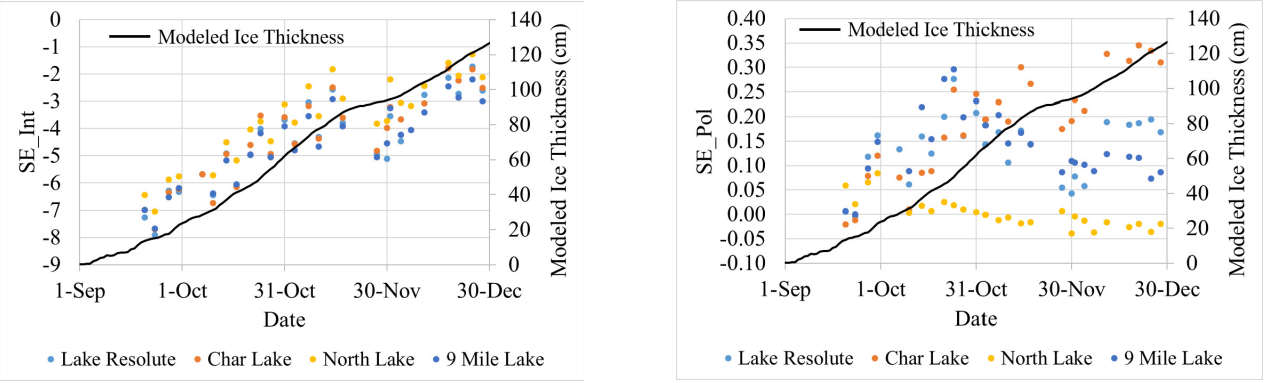

Fig. 7. Variation of the modeled ice thickness and (a) intensity and (b) polarimetric components of the Shannon entropy during the ice growth.

TABLE V
STATISTICS OF THE STOKES VECTOR ELEMENTS WITH THE P-VALUE OF ANOVA TEST

		Lake Resolute	Char Lake	North Lake	9 Mile Lake
SV0	Mean	0.0364	0.0390	0.0521	0.0325
	variance	0.0007	0.0008	0.0012	0.0004
	P-Value	0.079			
SV1	Mean	-0.00418	-0.00857	-0.00539	-0.00443
	variance	0.00002	0.00006	0.00003	0.00002
	P-Value	0.030			
SV2	Mean	-0.00268	-0.00507	-0.00737	-0.00351
	variance	0.00001	0.00003	0.00007	0.00002
	P-Value	0.019			
SV3	Mean	0.0171	0.0244	0.0074	0.0163
	variance	0.0002	0.0005	0.0001	0.0001
	P-Value	0.001			

previous CP parameters, they showed a regression tendency closer to second degree polynomial, rather than linear, where higher goodness-of-fit is achieved. The first SV0 and fourth SV3 elements show an increasing trend with lake ice growth [Fig. 6(a) and (d)]. The rate of variation is remarkably higher after 80 cm thick. It is worth noting that the increase in air temperature (mid to end of November) when ice thickness was about 90 cm caused a large drop in the values of SV0 and SV3. The high sensitivity of these two elements to change in snow caused by warm air temperature impedes their use as thickness indicators under this condition.

The second SV1 and third SV2 elements show an inverse relationship with lake ice growth [Fig. 6(b) and (c)] but not until the ice thickness reaches 40 cm. The consistently negative sign of the SV1 and SV2 elements, with few exceptions, indicates the presence of power in the linear polarized vertical and linear polarized 135° tilt components of the returned signal. These components are triggered by the surface scattering from the ice–water interface. The surface scattering mechanism should also be responsible for the positive sign of the SV3 element, with few exceptions, which implies power in the left-circular polarization component. This is expected since the transmitted radar signal is right-circular; and the surface scattering mechanism switches the circularity rotation.

We examine if the observed higher depolarization of the radar signal from North Lake depicted significant difference reflected in the Stokes elements. Table V presents the obtained p-value from the application of the ANOVA test for the case SV0. Given that the test yields a p-value $= 0.079 > 0.05$, the null hypothesis that the difference in the SV0 from the four lakes is not statistically significant is accepted. Therefore, the average expected total backscattering power from the four lakes does not differ significantly. As presented in Table V, the ANOVA test yields a p-value $= 0.030$ when applied for SV1, stating rejection of the null hypothesis that the difference in SV1 values between the four lakes is not statistically significant. We found that the p-value for this test becomes larger (0.854) than the significance level (0.05), accepting the null hypothesis, by excluding not only North Lake but also Char Lake. Therefore, only Lake Resolute and 9 Mile Lake reveals statistically insignificant difference in SV1. For SV2, the ANOVA test resulted in a p-value $= 0.019$ (<0.05), leading to the rejection of the null hypothesis (Table V). However, when excluding North Lake the null hypothesis of the ANOVA test is accepted with a p-value $= 0.141$. Finally, applying the ANOVA test to the SV3 yielded a rejection of the null hypothesis at a low p-value $= 0.001$. However, by excluding North Lake, the null hypothesis of the ANOVA test is accepted with a p-value $= 0.151$. Interesting to note that the SV3 values for North Lake is consistently lower than those from the other lakes for thicker ice >20 cm. This should be expected given that the SV3 element is linked to the average power received in circular polarization. The increased depolarization of the radar signal from the ice layer of North Lake decreases the average power in circular polarization.

TABLE VI
STATISTICS OF THE SHANNON ENTROPY WITH THE P-VALUE OF ANOVA TEST

		Lake Resolute	Char Lake	North Lake	9 Mile Lake
SE_Int	Mean	-4.5	-4.3	-3.7	-4.5
	variance	2.6	2.7	2.5	2.1
	P-Value	0.187			
SE_Pol	Mean	0.134	0.187	0.002	0.137
	variance	0.005	0.012	0.001	0.005
	P-Value	$1x10^{-13}$			

TABLE VII
STATISTICS OF THE REMAINING CP PARAMETERS WITH THE P-VALUE OF ANOVA TEST

		Lake Resolute	Char Lake	North Lake	9 Mile Lake
μ	Mean	0.40	0.50	0.13	0.45
	variance	0.02	0.04	0.01	0.01
	P-Value	$7x10^{-15}$			
m	Mean	0.53	0.62	0.41	0.54
	variance	0.008	0.023	0.001	0.007
	P-Value	$6x10^{-10}$			
ρ_{RHRV}	Mean	0.48	0.52	0.40	0.49
	variance	0.0027	0.0066	0.0005	0.0024
	P-Value	$3x10^{-10}$			
δ_{RHRV}	Mean	-76.4°	-83.9°	-35.2°	-91.3°
	variance	578.7	815.5	954.6	306.0
	P-Value	$5x10^{-12}$			
$\sigma^0_{RR}/\sigma^0_{RL}$	Mean	0.50	0.40	0.92	0.42
	variance	0.04	0.06	0.05	0.02
	P-Value	$6x10^{-16}$			
α_s	Mean	19.9°	18.6°	36.4°	16.7°
	variance	58.0	80.6	59.4	33.1
	P-Value	$4x10^{-16}$			

4) Shannon Entropy: The evolution of the intensity (SE_Int) and polarimetric (SE_Pol) components of the Shannon entropy are depicted in Fig. 7. Furthermore, Table VI presents statistics of the two components. SE_Int tends to increase with the lake ice growth. This tendency is expected since we have previously observed a similar increasing tendency with the SV0 element, which is a scaled value of SE_Int. However, the increasing tendency of the SE_Int with ice growth is nearly linear rather second-order polynomial. The effect of the increase in air temperature in November is also observed in Fig. 7(a). The application of the ANOVA test to SE_Int yields a p-value $= 0.187$, accepting the null hypothesis that the difference between the SE_Int values from the lakes is not statistically significant. This is expected since the null hypothesis was accepted for SV0.

Fig. 7(b) shows the variation of SE_Pol with ice growth. The SE_Pol depends on the Barakat degree of polarization [32]. Unlike SE_Int, SE_Pol does not generally reveal any trend with lake ice growth. The SE_Pol is characterized by a non-trivial variability within each lake, especially for Lake Resolute, Char Lake, and 9 Mile Lake, and between the four lakes. The variability of the SE_Pol should be associated with fluctuations of the contributions of the surface and the volume scattering mechanisms in the backscattered signal in each lake. The variability of the SE_Pol for North Lake is within a relatively narrow range, compared with the rest of the lakes. Moreover, North Lake presents the lowest SE_Pol values. This is expected given that North Lake uniquely presented a consistently higher volume scattering mechanism contribution relative to the surface scattering as previously discussed. We examine the difference between lakes in terms of SE_Pol parameters by applying the ANOVA test. Herein, the obtained p-value (1×10^{-13}) was small enough to reject the null hypothesis. The null hypothesis is accepted when it is applied to Lake Resolute and 9 Mile Lake (p-value $= 0.889$), excluding not only North Lake but also Char lake. These results are similar to the previously obtained results for the SV1.

5) Other CP Parameters:: In this subsection, all the remaining CP parameters from Table II are discussed and analyzed. In addition, statistics of these parameters are calculated and presented in Table VII. Fig. 8(a)–(c) shows evolution plots of the conformity coefficient (μ), the degree of polarization (m), and the RH and RV correlation (ρ_{RHRV}), respectively, with ice growth. We note that these three CP parameters have similar variability patterns for the four lakes, but at different scale, without revealing any specific tendency with the lake ice growth. This visually indicates high correlation of these three CP parameters.

The variability of μ for Lake Resolute, Char Lake, and 9 Mile Lake during the ice growth is higher than that of North Lake [Fig. 8(a)]. This should be associated with the alternating contributions of the volume and surface scattering mechanisms in the backscattering process during the ice growth. In contrast, North Lake with its constantly higher volume scattering mechanism is revealing much reduced variability due to the higher depolarization of the scattered radar signal. With exception of the very early ice growth (thickness < 15 cm), μ is consistently lowest for North Lake and closer to zero. The mean values

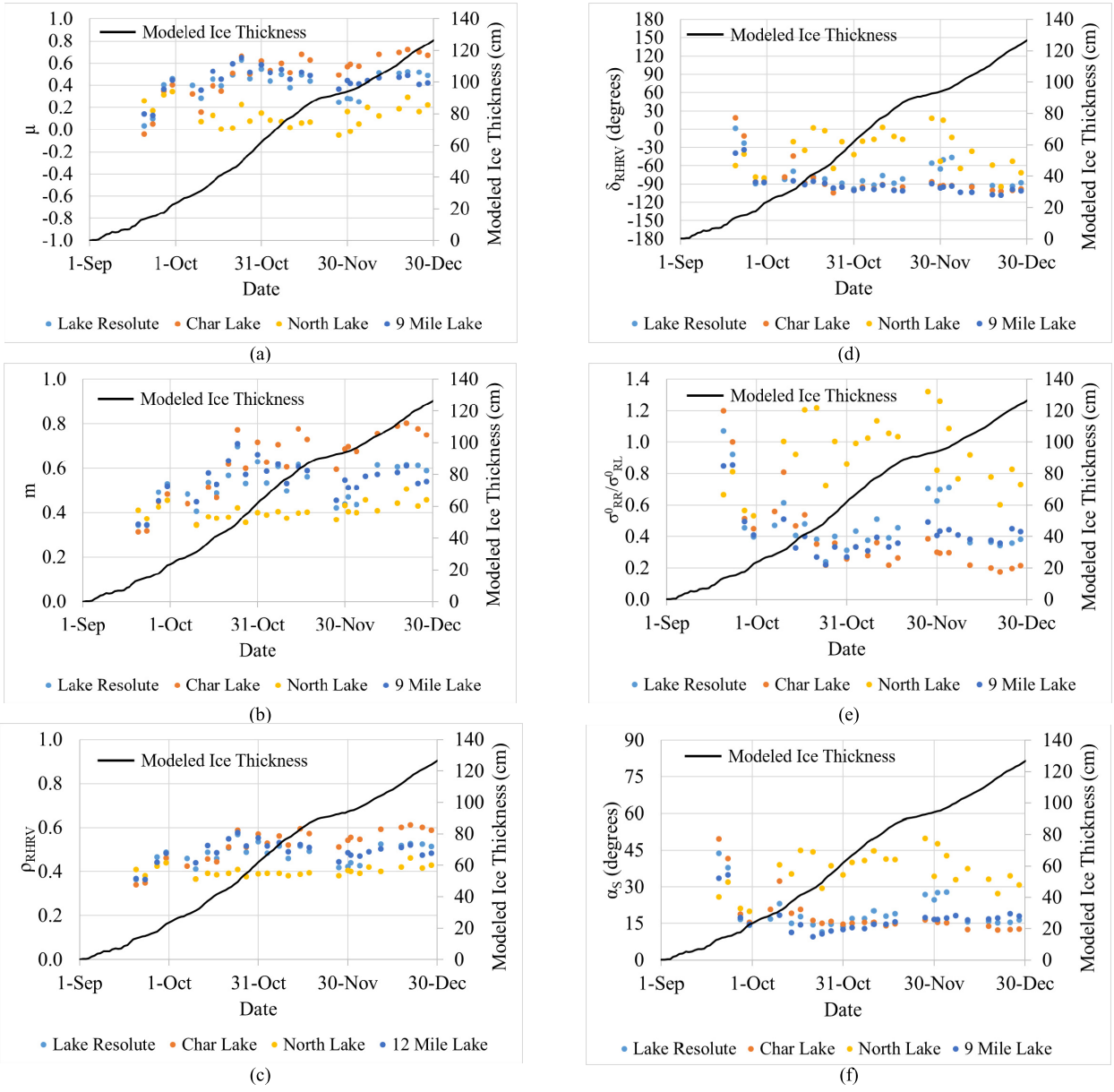

Fig. 8. Variation of modeled ice thickness and (a) μ, (b) m, (c) ρ_{RHRV}, (d) δ_{RHRV}, (e) $\sigma^0_{RR}/\sigma^0_{RL}$, and (f) α_s CP parameters during the ice growth.

of μ for North Lake is 0.13 confirming the dominance of the volume backscattering, while for the other lakes the mean of μ varies between 0.40 and 0.50 confirming the significant contribution of both volume and surface backscattering (Table VII). The fact that no observations for $\mu < 0$ confirms the insignificant contribution of the double-bounce scattering mechanism [Fig. 8(a)]. The observed variability of μ for the four lakes is also depicted in m and ρ_{RHRV} [Fig. 8(b) and (c)]. North Lake has the lowest values of m and ρ_{RHRV}, with mean values 0.41 and 0.40, respectively (Table VII). We apply the ANOVA test to statistically evaluate the significance of the difference in these three parameters between the four lakes. As shown in Table VII, the test yields very low p-value, rejecting the null hypothesis for μ, m, and ρ_{RHRV}. The null hypothesis is accepted by repeating the test after the exclusion of North Lake for μ (p-value = 0.109) and ρ_{RHRV} (p-value = 0.081). This confirms the remarkable difference of North Lake compared with the other lakes in these two parameters. However, this is not the case for the m parameter, where the null hypothesis is accepted once North Lake and Char Lake are excluded (p-value = 0.449). The achieved test results of m are similar to those which we previously obtained for SV1 and SE_Pol.

Fig. 8(d)–(f) shows evolution plots of the RH and RV phase difference (δ_{RHRV}), the circular polarization ratio ($\sigma^0_{RR}/\sigma^0_{RL}$), and the alpha angle ($\alpha_s$), respectively. Besides, Table VII presents statistics of these parameters including the mean and the variance for each lake. As shown in Fig. 8(d)–(f), these three CP parameters should be highly correlated given that they expose nearly similar variability patterns for the four lakes, once again, at different scale. However, they do not reveal any trend with lake ice growth. The δ_{RHRV} parameter for Lake Resolute, Char Lake, and 9 Mile Lake is characterized by a reduced variability [Fig. 8(d)] and quite close values

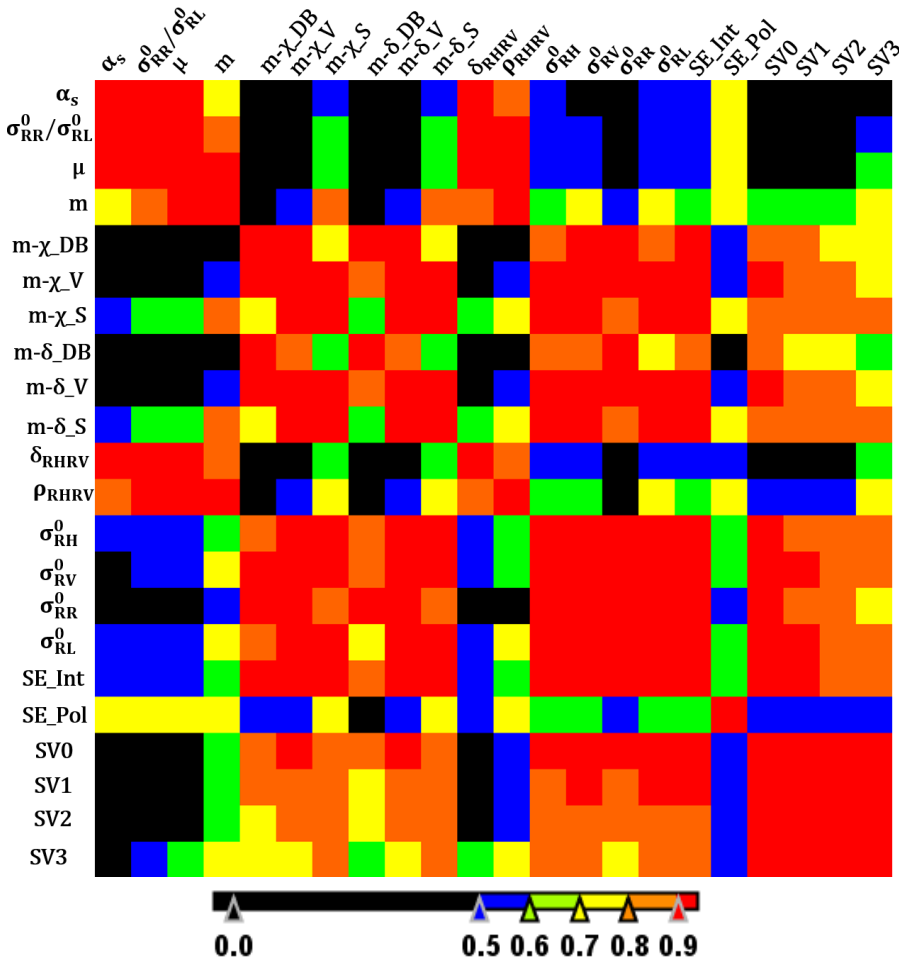

Fig. 9. Correlation of the CP parameters.

during the ice growth with a mean value ranging between $-76.4°$ for Lake Resolute and $-91.3°$ for 9 Mile Lake (Table VII). This is not the case for North Lake, where δ_{RHRV} values remarkably fluctuate above the δ_{RHRV} values of the other three lakes [Fig. 8(d)], with a mean value of $-35.2°$. This should illustrate the characteristic higher volume scattering of North Lake. A similar behavior is presented by the $\sigma^0_{RR}/\sigma^0_{RL}$ and α_s parameters [Fig. 8(e) and (f)]. It is worth noting that $\sigma^0_{RR}/\sigma^0_{RL}$ for North Lake has achieved a considerably higher mean value (0.92) compared with the other lakes (Table VII). This should be expectable since σ^0_{RR} is highly correlated with the volume scattering mechanism [6]. Therefore, the consistent higher volume scattering in the case of North Lake triggered a higher σ^0_{RR} values, which increases the $\sigma^0_{RR}/\sigma^0_{RL}$ parameter for this lake. Our findings are also depicted by α_s parameter, as shown in Fig. 8(f). Once again, North Lake is characterized by medium values of α_s with a mean value of 36.4° (Table VII), confirming the observed consistent higher volume scattering. The other three lakes are characterized by lower α_s values with mean values between 16.7° (9 Mile Lake) and 19.9° (Lake Resolute), indicating the significant presence of surface scattering mechanism.

As presented in Table VII, the application of the ANOVA test to δ_{RHRV}, $\sigma^0_{RR}/\sigma^0_{RL}$, and α_s yields very low p-values which state the rejection of the null hypothesis since the mean value of at least one lake is statistically different. By excluding North Lake, the null hypothesis of the ANOVA test is accepted with p-value $= 0.083$, 0.210, and 0.317 for δ_{RHRV}, $\sigma^0_{RR}/\sigma^0_{RL}$, and α_s, respectively.

It is interesting to note that the ρ_{RHRV}, m, and μ parameters form a group of CP parameters opposite to a group containing the δ_{RHRV}, $\sigma^0_{RR}/\sigma^0_{RL}$, and α_s parameters in the sense that the former is characterized by higher variability for the Resolute Lake, Char Lake, and 9 Mile Lake, but lower for North Lake, while the latter is characterized by an opposite behavior. This clearly indicates the different sensitivity of these two groups.

C. Correlation of CP Parameters

Herein, we briefly analyze the correlation of the CP parameters. Fig. 9 shows the average correlation of these parameters from the four lakes. CP parameters with absolute correlation <0.5 appear in black. As shown in Fig. 9, most of the CP parameters reveal an absolute correlation >0.5. Interestingly, some CP parameters are highly correlated. An example is the backscattering coefficients σ^0_{RH}, σ^0_{RV}, σ^0_{RR}, and σ^0_{RL} with absolute correlation >0.9. These parameters are also highly correlated with the volume scattering mechanism (m-χ_V and m-δ_V), SE_Int, and SV0. It is worth noting the very high correlation (>0.9) of the σ^0_{RH}, σ^0_{RV}, and σ^0_{RL} with

the surface scattering mechanism (m-χ_S and m-δ_S). The correlation of σ^0_{RR} with the surface scattering mechanism is still high, but <0.9 (between 0.8 and 0.9). This should be associated with the fact that σ^0_{RR} is characterized by increased contribution (doubled) of cross-polarization (RR = 0.5(HH – VV – 2jHV)), unlike σ^0_{RH}, σ^0_{RV}, and σ^0_{RL} [33].

Our previous assumption of high correlation of μ, m, and ρ_{RHRV} parameters which were found to exhibit similar variability pattern is confirmed, since these three parameters achieved a correlation >0.9. Similar correlation results are obtained for δ_{RHRV}, $\sigma^0_{RR}/\sigma^0_{RL}$, and α_s, which were also found to exhibit similar variability pattern. Given that SV0 is a scaled value of SE_Int, their correlation is equal to 1. The correlation of m-χ_V and m-δ_V is also equal to 1, given that they are estimated from identical mathematical formula. Interestingly, none of the CP parameters presents an absolute correlation <0.5 with all the others.

V. Conclusions and Recommendations

In this study, we explore potential interpretation of CP SAR parameters in relation to the thermodynamic development of lake ice thickness. Such a study is necessary to investigate the impacts of climate change on high-latitude lakes, such as ice growth rate, maximum ice thickness, and onset of freezing and break-up. CP SAR configuration is selected because of the enhanced radar target information over a wide spatial coverage. Sensitivity of 22 CP parameters to the thickness during the early ice growth was investigated. Data were obtained for four lakes selected in Cornwallis Island, Canadian Central Arctic. The study period was from early ice formation in September 2017 until the ice matured by the end of December 2017. Thermodynamically grown lake ice was estimated using established and commonly used empirical model.

This study focused on the trends of the CP parameters and their links to lake ice growth with physical explanation. To this end, we found that most of the examined CP parameters exhibited correlation with lake ice growth likely triggered by the increase in two ice properties: the air bubbles within the ice layer and the ice–water interface roughness. All backscattering coefficient parameters (σ^0_{RH}, σ^0_{RV}, σ^0_{RR}, and σ^0_{RL}) exhibit linear increasing tendency with ice growth. This indicates that a single-polarized SAR system could be sufficient for retrieval of lake ice growth information instead of dual CP SAR system. To this end, a better understanding of how varying ice properties impact SAR signals is required. A similar behavior was observed from surface and volume scattering mechanisms obtained from both m-χ and m-δ decomposition methods, which constitute the dominant scattering mechanisms from lake ice. Unlike the polarimetric component of the Shannon entropy (SE_Pol), the intensity component (SE_Int) showed also a linear increase with the lake ice growth. Remarkably, all the four elements of the Stokes vector seem to exhibit a tendency with lake ice growth. However, unlike the other CP parameters, these elements show a tendency closer to second degree polynomial, rather than linear, where higher goodness-of-fit is achieved.

The only effect of snow observed in the CP SAR parameters was when air temperature increased between mid and end of November to approach −4 °C, since snow must have acquired wetness. This increase in the snow wetness caused a reduction in the values of the CP parameters showing sensitivity to lake ice growth. This is valid for all parameters, including the second (SV1) and the third (SV2) elements of the Stokes vector since the negative sign of these two elements is an indication of the direction of the polarization (horizontal or vertical) and the tilt angle (45° or 134°), respectively.

North Lake uniquely showed increasing volume scattering contribution in the backscattering signal relatively to all the other examined lakes. We postulate that the increasing volume scattering is triggered by higher density of air bubbles due to higher gas production activities. This assumption is adopted following results from field measurements in the area conducted during previous studies which identified North Lake as a lake with much higher concentration of nitrite and nitrate. The significance of this increase in volume scattering was statistically evaluated in all CP parameters using the ANOVA test. Through this test, the impact of North Lake higher density of air bubbles was statistically revealed in a number CP parameters. However, not all of these parameters present a specific trend with ice growth. Despite the statistically significant difference of the volume scattering from North Lake as the ANOVA test unveiled, the difference of surface scattering between lakes remained statistically insignificant. The increased density of air bubbles in North Lake should have also enhanced the presence of columnar air bubbles, which subsequently increased the chances for double-bounce scattering. Though secondary, double-bounce scattering proved by the ANOVA test statistically different from North Lake compared with the other lakes. Our findings for North Lake could shed the light on a new application of SAR remote sensing for monitoring inorganic nitrogen such as nitrite and nitrate in northern lakes. Such application needs to be further evaluated in a separate future study over a number of lakes, with field measurements prior the onset of freezing. A brief correlation analysis of the CP parameters was also performed. We found that most of the CP parameters expose an absolute correlation >0.5. A considerable number of CP parameters presented a correlation >0.9, indicating mutual information about the lake ice properties.

Including real CP SAR data from RCM was not possible, given that the mission declared operational at the end of December 2019, after the required study period. However, it is expected to confirm our findings with real RCM CP SAR data in a future research work.

Acknowledgment

The authors would like to thank Dean Flett of the Canadian Ice Service (CIS) for endorsing this project and Benjamin Deschamps and Celine Fabi of CIS for the scene selection and acquisition of Radarsat-2 data. Wayne Davidson from the Upper Air Network of Environment and Climate Change Canada at Resolute Bay provided information on the lakes status during the study period. Furthermore, the authors would like to thank Dr. Derek Muir, Dr. Günter Köck, and Dr. Scott Lamoureux for the valuable information they provided about the lakes in the study area from past field campaigns. The

authors thank Dr. François Charbonneau and the Canada Centre for Mapping and Earth Observation for providing the CP SAR simulator. Finally, the authors would like to thank the anonymous reviewers for their constructive comments which have greatly improved the manuscript. RADARSAT-2 Data and Products ©Maxar Technologies Ltd. (2018)—All Rights Reserved. RADARSAT is an official mark of the Canadian Space Agency.

REFERENCES

[1] G. Seguin and S. Ahmed, "RADARSAT constellation, project objectives and status," in *Proc. IEEE Int. Geosci. Remote Sens. Symp.*, Cape Town, South Africa, Jul. 2009, pp. II-894–II-897.

[2] R. K. Raney, "Hybrid-polarity SAR architecture," *IEEE Trans. Geosci. Remote Sens.*, vol. 45, no. 11, pp. 3397–3404, Nov. 2007.

[3] F. J. Charbonneau *et al.*, "Compact polarimetry overview and applications assessment," *Can. J. Remote Sens.*, vol. 36, pp. S298–S315, Jan. 2010.

[4] M. Dabboor and T. Geldsetzer, "Towards sea ice classification using simulated RADARSAT constellation mission compact polarimetric SAR imagery," *Remote Sens. Environ.*, vol. 140, pp. 189–195, Jan. 2014.

[5] M. Dabboor, S. Iris, and V. Singhroy, "The RADARSAT constellation mission in support of environmental applications," *Proceedings*, vol. 2, no. 7, p. 323, Mar. 2018.

[6] T. Geldsetzer, M. Arkett, T. Zagon, F. Charbonneau, J. J. Yackel, and R. K. Scharien, "All-season compact-polarimetry C-band SAR observations of sea ice," *Can. J. Remote Sens.*, vol. 41, no. 5, pp. 485–504, Sep. 2015.

[7] M. Espeseth, C. Brekke, and A. Johansson, "Assessment of RISAT-1 and Radarsat-2 for sea ice observations from a hybrid-polarity perspective," *Remote Sens.*, vol. 9, no. 11, p. 1088, Oct. 2017.

[8] M. Dabboor, S. Singha, B. Montpetit, B. Deschamps, and D. Flett, "Pre-launch assessment of RADARSAT constellation mission medium resolution modes for sea oil slicks and lookalike discrimination," *Can. J. Remote Sens.*, vol. 45, nos. 3–4, pp. 530–549, Jul. 2019.

[9] M. M. Espeseth, S. Skrunes, C. E. Jones, C. Brekke, B. Holt, and A. P. Doulgeris, "Analysis of evolving oil spills in full-polarimetric and hybrid-polarity SAR," *IEEE Trans. Geosci. Remote Sens.*, vol. 55, no. 7, pp. 4190–4210, Jul. 2017.

[10] X. Wang, Y. Shao, F. Zhang, and W. Tian, "Comparison of C- and L-band simulated compact polarized SAR in oil spill detection," *Frontiers Earth Sci.*, vol. 13, no. 2, pp. 351–360, Jun. 2019.

[11] M. Dabboor, L. White, B. Brisco, and F. Charbonneau, "Change detection with compact polarimetric SAR for monitoring wetlands," *Can. J. Remote Sens.*, vol. 41, no. 5, pp. 408–417, Oct. 2015.

[12] M. Dabboor *et al.*, "Comparison of compact and fully polarimetric SAR for multitemporal wetland monitoring," *IEEE J. Sel. Topics Appl. Earth Observ. Remote Sens.*, vol. 12, no. 5, pp. 1417–1430, May 2019.

[13] T. Geldsetzer, F. Charbonneau, M. Arkett, and T. Zagon, "Ocean wind study using simulated RCM compact-polarimetry SAR," *Can. J. Remote Sens.*, vol. 41, no. 5, pp. 418–430, Sep. 2015.

[14] T. Geldsetzer, S. K. Khurshid, K. Warner, F. Botelho, and D. Flett, "Wind speed retrieval from simulated RADARSAT constellation mission compact polarimetry SAR data for marine application," *Remote Sens.*, vol. 11, no. 14, p. 1682, Jul. 2019.

[15] H. Li, J. Wu, W. Perrie, and Y. He, "Wind speed retrieval from hybrid-pol compact polarization synthetic aperture radar images," *IEEE J. Ocean. Eng.*, vol. 43, no. 3, pp. 713–724, Jul. 2018.

[16] M. J. Collins, M. Ma, and M. Dabboor, "On the effect of polarization and incidence angle on the estimation of significant wave height from SAR data," *IEEE Trans. Geosci. Remote Sens.*, vol. 57, no. 7, pp. 4529–4543, Jul. 2019.

[17] X. Wang, Y. Shao, L. She, W. Tian, K. Li, and L. Liu, "Ocean wave information retrieval using simulated compact polarized SAR from Radarsat-2," *J. Sensors*, vol. 2018, pp. 1–12, Jun. 2018, 1738014.

[18] F. Pang, "RADARSAT-2 polarimetric radar imaging for lake ice mapping," M.S. thesis, Dept. Geogr., Univ. Waterloo, Waterloo, ON, Canada, 2017.

[19] M. Engram, C. D. Arp, B. M. Jones, O. A. Ajadi, and F. J. Meyer, "Analyzing floating and bedfast lake ice regimes across arctic Alaska using 25 years of space-borne SAR imagery," *Remote Sens. Environ.*, vol. 209, pp. 660–676, May 2018.

[20] J. Wang, C. Duguay, D. Clausi, V. Pinard, and S. Howell, "Semi-automated classification of lake ice cover using dual polarization RADARSAT-2 imagery," *Remote Sens.*, vol. 10, no. 11, p. 1727, Nov. 2018.

[21] D. K. Atwood, G. E. Gunn, C. Roussi, J. Wu, C. Duguay, and K. Sarabandi, "Microwave backscatter from arctic lake ice and polarimetric implications," *IEEE Trans. Geosci. Remote Sens.*, vol. 53, no. 11, pp. 5972–5982, Nov. 2015.

[22] G. E. Gunn, C. R. Duguay, D. K. Atwood, J. King, and P. Toose, "Observing scattering mechanisms of bubbled freshwater lake ice using polarimetric RADARSAT-2 (C-band) and UW-scat (X- and ku-bands)," *IEEE Trans. Geosci. Remote Sens.*, vol. 56, no. 5, pp. 2887–2903, May 2018.

[23] B. Tian *et al.*, "Characterizing C-band backscattering from thermokarst lake ice on the Qinghai–Tibet plateau," *ISPRS J. Photogramm. Remote Sens.*, vol. 104, pp. 63–76, Jun. 2015.

[24] S. V. Nghiem and G. A. Leshkevich, "Satellite SAR remote sensing of great lakes ice cover, part 1. Ice backscatter signatures at C band," *J. Great Lakes Res.*, vol. 33, no. 4, pp. 722–735, Dec. 2007.

[25] J. J. van der Sanden, T. Geldsetzer, H. Drouin, and A. Deschamps, "On the anticipated utility of RCM CP data for freshwater ICE mapping and monitoring," in *Proc. IEEE Geosci. Remote Sens. Symp.*, Quebec City, QC, Canada, Jul. 2014, pp. 1564–1567.

[26] J. J. van der Sanden and T. Geldsetzer, "Compact polarimetry in support of lake ice breakup monitoring: Anticipating the RADARSAT constellation mission," *Can. J. Remote Sens.*, vol. 41, no. 5, pp. 440–457, Sep. 2015.

[27] G. L. Lescord, K. A. Kidd, J. L. Kirk, N. J. O'Driscoll, X. Wang, and D. C. G. Muir, "Factors affecting biotic mercury concentrations and biomagnification through lake food webs in the Canadian high arctic," *Sci. Total Environ.*, vols. 509–510, pp. 195–205, Mar. 2015.

[28] J. J. Goering and V. A. Dugdale, "Estimates of the rates of denitrification in a subarctic lake," *Limnol. Oceanogr.*, vol. 11, no. 1, pp. 113–117, 1966.

[29] R. K. Raney, J. T. S. Cahill, G. W. Patterson, and D. B. J. Bussey, "The m-chi decomposition of hybrid dual-polarimetric radar data with application to lunar craters," *J. Geophys. Res., Planets*, vol. 117, no. E12, Dec. 2012.

[30] J. S. Lee and E. Pottier, *Polarimetric Radar Imaging: From Basics to Applications*. Boca Raton, FL, USA: CRC Press, 2009.

[31] P. Réfrégier and J. Morio, "Shannon entropy of partially polarized and partially coherent light with Gaussian fluctuations," *J. Opt. Soc. Amer. A, Opt. Image Sci.*, vol. 23, no. 12, pp. 3036–3044, 2006.

[32] S. R. Cloude, D. G. Goodenough, and H. Chen, "Compact decomposition theory," *IEEE Geosci. Remote Sens. Lett.*, vol. 9, no. 1, pp. 28–32, Jan. 2012.

[33] M.-L. Truong-Loi, A. Freeman, P. C. Dubois-Fernandez, and E. Pottier, "Estimation of soil moisture and Faraday rotation from bare surfaces using compact polarimetry," *IEEE Trans. Geosci. Remote Sens.*, vol. 47, no. 11, pp. 3608–3615, Nov. 2009.

[34] G. R. Iversen and H. Norpoth, *Quantitative Applications in the Social Sciences: Analysis of Variance*. Thousand Oaks, CA, USA: SAGE Publications, Inc. 1987.

[35] G. D. Ashton, "Thin ice growth," *Water Resour. Res.*, vol. 25, no. 3, pp. 564–566, Mar. 1989.

[36] M. Shokr and M. Dabboor, "Observations of SAR polarimetric parameters of lake and fast sea ice during the early growth phase," *Remote Sens. Environ.*, vol. 247, Sep. 2020, Art. no. 111910.

[37] F. Ulaby, R. K. Moore, and A. K. Fung, *Microwave Remote Sensing: Radar Remote Sensing and Surface Scattering and Emission Theory*, vol. 2. Norwood, MA, USA: Artech House, 1982.

[38] D. W. Schindler, H. E. Welch, J. Kalff, G. J. Brunskill, and N. Kritsch, "Physical and chemical limnology of char lake, Cornwallis island (75° n Lat)," *J. Fisheries Res. Board Canada*, vol. 31, no. 5, pp. 585–607, May 1974.

[39] Y.-S. Kim, R. Onstott, and R. Moore, "Effect of a snow cover on microwave backscatter from sea ice," *IEEE J. Ocean. Eng.*, vol. 9, no. 5, pp. 383–388, Dec. 1984.

[40] M. Shokr, and N. K. Sinha, *Sea Ice: Physics and Remote Sensing, Geophysical Monograph*, vol. 209. Hoboken, NJ, USA: Wiley, 2015.

[41] G. D. Ashton, *River and Lake Ice Engineering*, Highlands Ranch, CO, USA: Water Resources Publications, 2004.

[42] W. F. Weeks, *On Sea Ice*. Fairbanks, AK, USA: Univ. Alaska Press, 2010.

[43] W. F. Weeks, A. G. Fountain, M. L. Bryan, and C. Elachi, "Differences in radar return from ice-covered north slope lakes," *J. Geophys. Res. Oceans*, vol. 83, no. C8, pp. 4069–4073, 1978.

Mohammed Dabboor (Member, IEEE) received the B.Sc. and M.Sc. degrees in geomatics engineering from the National Technical University of Athens, Athens, Greece, in 2003 and 2005, respectively, and the Ph.D. degree in spaceborne synthetic aperture radar (SAR) remote sensing from the University of Calgary, Calgary, AB, Canada, in 2010.

He worked as a Natural Sciences and Engineering Research Council of Canada (NSERC) Post-Doctoral Visiting Fellow with the Science and Technology Branch, Environment and Climate Change Canada, Government of Canada, until February 2015. After his post-doctoral studies, he joined the NASA Marshall Space Flight Center (MSFC), Huntsville, AL, USA, as an Interim Research Scientist until August 2015. Since September 2015, he has been a Research Scientist with the Science and Technology Branch, Environment and Climate Change Canada, Government of Canada. He leads the research in various projects of the Canadian Space Agency (CSA) related to the RADARSAT Constellation Mission (RCM). His research interests include the analysis of fully and compact polarimetric SAR imagery and spaceborne SAR mission design.

Dr. Dabboor is a member of the CSA User and Science Team of the RCM and the CSA working group for the calibration and validation of the SWOT satellite mission. He acts as a Canada Representative in the international Group on Earth Observations (GEO)—Climate Change working group. He is the recipient of a number of awards, such as the Queen Elizabeth II Graduate Award, the Helmut Moritz Graduate Award, and the Canadian Geophysical Union Geodesy Section Best Student Paper Award in 2007.

Mohammed Shokr (Senior Member, IEEE) received the Ph.D. degree in aeronautical engineering from Cairo University, Cairo, Egypt, in 1980.

In 1989, he started his research on sea ice physics and remote sensing to support the national operational sea ice monitoring program in Canada. He participated in many field trips to different locations in the Arctic to study ice and snow properties in relation to remote sensing observations. From 2016 to 2019, he was a Visiting Professor with Beijing Normal University, Beijing, China, and Wuhan University, Wuhan, China, where he taught graduate courses on sea ice physics and remote sensing and continued his research on impact of climate change on polar sea ice. His research interests included physics of sea ice and snow, retrieval of sea ice parameters from remote sensing observations, especially imaging radar, and sea ice climatology in the polar regions.